Unsupervised Cell Nuclei Segmentation Based on Morphology and Adaptive Active Contour Modelling

Ziming Zeng[1,2], Harry Strange[2], Chunlei Han[3], and Reyer Zwiggelaar[2]

[1] Information and Control Engineering Faculty,
Shenyang Jianzhu University, Liaoning, China
[2] Department of Computer Science, Aberystwyth University, UK
[3] Turku PET Center, Turku University Hospital, Finland

Abstract. This paper proposes an unsupervised segmentation scheme for cell nuclei. This method computes the cell nuclei by using adaptive active contour modelling which is driven by the morphology method. Firstly, morphology is used to enhance the gray level values of cell nuclei. Then binary cell nuclei is acquired by using an image subtraction technique. Secondly, the masks of cell nuclei are utilized to drive an adaptive region-based active contour modelling to segment the cell nuclei. In addition, an artificial interactive segmentation method is used to generate the ground truth of cell nuclei. This method can have an interest in several applications covering different kinds of cell nuclei. Experiments show that the proposed method can generate accurate segmentation results compared with alternative approaches.

Keywords: Cell Nuclei, Morphology, Adaptive Active Contour Modelling, Segmentation, Ground Truth.

1 Introduction

Cell nuclei segmentation is a fundamental topic of quantitative analysis of cytology and histology images. The accurate segmentation of the cell nuclei plays an important role for detection of the pathological type, developing radiation treatment planning, and quantitative measurement. Clinically, people tend to recognize the cell nuclei by analysing the boundary, location and texture information. Many methods are used successfully for cell nuclei segmentation, for examlpe: data-driven methods (such as thresholding [1]), machine learning method (such as neural network [2]), mathematical morphology methods (such as morphology opening and closing [3]), and deformable contours (such as snakes [4]). In these methods, Tophat [5] which is a classic morphology method is widely used to detect the boundaries of cell nuclei. However, due to the diversity of the structures contained in the images, the intense variation of background caused by uneven staining and overlapping cell nuclei leads to the fact that cell nuclei boundaries in the segmentation results are not always convex. In addition, a reasonable threshold for generating binary cell nuclei is difficult to be obtained.

M. Kamel and A. Campilho (Eds.): ICIAR 2013, LNCS 7950, pp. 605–612, 2013.

Some people have tried to use deformable contour techniques for cell nuclei image analysis [6], which can result in smooth, plausible outlines. Zhang et al. [7] developed a coupled geometric active contour to track cell nuclei. Yang et al. [8] investigated a robust color gradient vector flow active contour model to segment cell nuclei. Li et al. [9] developed the region based an energy fitting function by introducing a Gaussian kernel, which can effectively deal with the noise and density inhomogenity. Yang et al. [10] introduced a split Bregman technique [11] to improve the computing speed when minimizing the data energy fitting function. However, some state-of-art active contour methods are still highly dependent on initialization and lack of adaptiveness. With respect to these problems, an adaptive active contour modelling combined with morphology is proposed to segment the cell nuclei.

2 Methodology

The proposed method has two steps. In the first step, morphology is used to enhance the cell nuclei. Then the enhanced image is converted to a binary image and the grey level values corresponding to the binary cell nuclei are used to estimate parameters. In the second step, improved active contour modelling is used to segment the cell nuclei.

2.1 Cell Nuclei Enhancement and Parameter Estimation

In this step, the color image (see Fig. 1a) is converted to a grey level image (see Fig. 1b). Morphological opening and closing [12] is performed on the grey level image (see Fig. 1c and Fig. 1e) with circular structuring elements. The aim of the opening and closing is to smooth the outlines, and weaken the narrow parts which denote cell nuclei. Subsequently, the cell nuclei is enhanced by subtracting the original image (see Fig. 1d and Fig. 1f). The cell nuclei is further enhanced by subtracting the two enhanced images (see Fig. 1g). In Fig. 1g, some pixel values are negative after substraction, we remove these pixels and a binary image is generated. Finally, small gaps surrounded by the white pixels are filled by using morphology. The final results are shown in Fig. 1h.

From the segmentation results, we can see the image substraction technique by using morphology can effectively segment the cell nuclei. However, this method fails to consider the density inhomogenity within the cell nuclei. The boundaries of most cell nuclei are not closed because of the density inhomogenity within the cell nuclei. In order to overcome this shortcoming, an improved active contour modelling is used to further refine the segmentation results. In this work, the morphology segmentation result is used to estimate some parameters in the active contour modelling. Specifically, the generated binary result is used as a mask to extract the corresponding grey level values of the pixels in Fig. 1b. Then the average of the grey level values $\mu_{cellnuclei}$ and the standard deviations $\sigma_{cellnuclei}$ is calculated within the mask region.

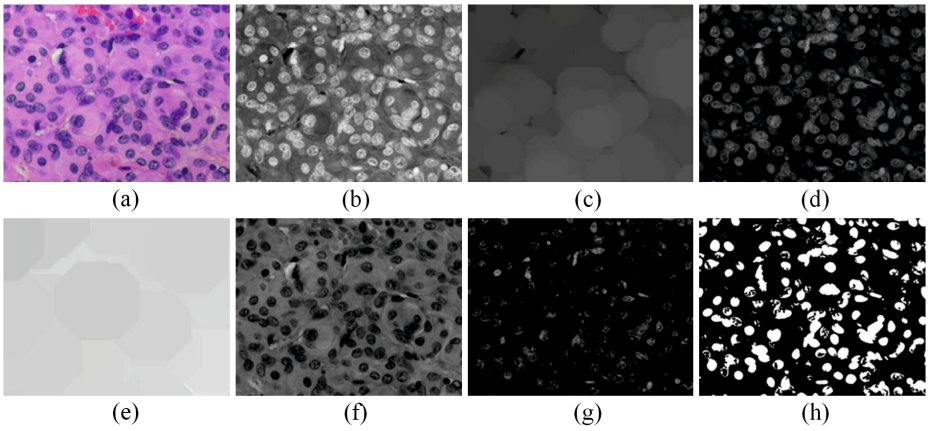

Fig. 1. Examples of morphology segmentation. (a) Original image, (b) grey level image after image inverting, (c) morphological opening, (d) subtracted image (the original image in (b) subtract from the morphological opening image in (c)), (e) morphological closing, (f) subtracted image (the morphological closing image in (c) subtract from the original image in (b)), (g) subtracted image (the enhanced image in (d) subtract from the enhanced image in (f)), (h) binary image.

2.2 Adaptive Active Contours Modelling

The active contour modelling which can perform well on noisy and density inhomogenity images is used to further refine the segmentation results. A region-based active surface model [9] and a global convex segmentation model [13] are used to obtain an energy function that can be minimized by convex optimization. Subsequently, the energy function is minimized along with the deformation of the contour using a Split Bregman technique [14,10]. As in [9,10], the energy function is defined as

$$E(\phi, f_1, f_2) = \varepsilon(\phi, f_1, f_2) + \mu P(\phi) \tag{1}$$

where ϕ denotes the contour of cell nuclei, the level set regularization term is defined as $P(\phi) = \int \frac{1}{2}(\mid \nabla\phi(x) \mid -1)^2 dx$. The region-scalable energy fitting function is defined as

$$\varepsilon(\phi, f_1(x), f_2(x)) = \sum_{i=1}^{2} \lambda_i \int K_\sigma(x-y) \mid f_i(x) - I(y) \mid^2 M_i(\phi(y)) dy \tag{2}$$

where $K_\sigma(u) = (1/(2\pi\sigma^2))e^{-|u|^2/2\sigma^2}$ is a Gaussian kernel. The local fitting energy ε is determined by the value of σ. The larger the value of σ, the greater the ability to handle noise and density inhomogenity at a large scale. However, a large value of σ might affect the segmentation accuracy. In this work, σ is automatic estimated as $\sigma = \langle k \times \sigma_{cellnuclei} \rangle$, where k is a constant value, $\langle \cdot \rangle$ is a rounding up function. In Eq. 2, $M_1(\phi) = H(\phi), M_2(\phi) = 1 - H(\phi)$. The

Heaviside function H is usually approximated by a smooth function $H_\varepsilon(x) = (1/2)[1 + (2/\pi)arctan(x/\xi)]$. In order to make the energy function adapt to different kinds of cell nuclei, we changed this function to:

$$H_\varepsilon(x) = \frac{1}{2}\left[1 + \frac{2}{\pi}arctan\left(\frac{x-T}{\xi}\right)\right] \tag{3}$$

where T is changeable according to the grey level of the segmented cell nuclei in the previous step, which is defined as

$$T = \frac{\mu_{cellnuclei} - \sigma_{cellnuclei}}{255} \tag{4}$$

According to the derivation written by Li et al. [9], the optimal functions $f_1(x)$, $f_2(x)$ that minimize $E(\phi, f_1, f_2)$ are obtained by:

$$f_i(x) = \frac{K_\sigma(x) * [M_i^\varepsilon(\phi(x))I(x)]}{K_\sigma(x) * M_i^\varepsilon(\phi(x))}, i = 1, 2 \tag{5}$$

For fixed $f_1(x)$, $f_2(x)$, the function ϕ is determined by

$$\frac{\partial\phi}{\partial t} = -\delta(\phi)(\lambda_1 e_1 - \lambda_2 e_2) - div(\frac{\nabla\phi}{\mid \nabla\phi \mid}) \tag{6}$$

where δ is the derivative of H_ε. $e_i(x) = \int K_\sigma(y-x) \mid I(x) - f_i(y) \mid_2 dy, i = 1, 2$. The simplified flow represents the gradient descent for minimizing the energy:

$$E(\phi) = \mid \nabla\phi \mid_1 + \langle\phi \cdot r\rangle, \tag{7}$$

where $r = \lambda_1 e_1 - \lambda_2 e_2$. Yang et al. [10] restricted the solution to lie in a finite interval in order to transform the constrained optimization problem to an unconstrained one. In this work, we constrain ϕ as $0 \leq \phi \leq 1$, which can guarantee a unique global minimal. The global convex model can be written as $min_{0\leq\phi\leq1}E(\phi) = min_{0\leq\phi\leq1}(\mid \nabla\phi \mid_1 + \langle\phi \cdot r\rangle)$. In [10], the minimization problem was written as $min_{0\leq\phi\leq1}E(\phi) = min_{0\leq\phi\leq1}(\mid \nabla\phi \mid_g + \langle\phi \cdot r\rangle)$.

Yang et al. [10] used the Split Bregman algorithm to solve the global convex model. The Split Bregman algorithm for minimizing the above function can be summarized as follows:

1: while $\parallel \phi^{k+1} - \phi^k \parallel > \Psi$ do
2: Define $r^k = \lambda_1 e_1^k - \lambda_2 e_2^k$
3: $\phi^{k+1} = GS(r^k, \overrightarrow{d^k}, \overrightarrow{b^k}, \lambda)$
4: $\overrightarrow{d}^{k+1} = shrink_g(\overrightarrow{b^k} + \nabla\phi^{k+1}, 1/\lambda)$
5: $\overrightarrow{b}^{k+1} = \overrightarrow{b}^k + \nabla\phi^{k+1} - \overrightarrow{d}^{k+1}$
6: Find $\Omega^k = \{x : \phi^k(x) > \mu\}$
7: Update e_1^k and e_2^k
8: end while,

where $GS(r^k, \overrightarrow{d^k}, \overrightarrow{b^k}, \lambda)$ denotes the Gauss-Seidal iteration method, $\overrightarrow{b}, \overrightarrow{d}$ are auxiliary variables, k is the iteration number, $shrink_g$ is a shrinkage frame (see [10]), and Ω is the segmented region. When the optimal ϕ is found, we can find the cell nuclei $\Omega^k = \{x : \phi^k(x) > 0.5\}$.

3 Experiment

Due to the limited histology images and meningioma subtypes, only five meningioma (meningotheliomatoes subtype) images (resolution 1300×1030 pixels) are used to evaluate our method. The ground truth segmentations were estimated using an artificial interactive segmentation method.

Fig. 2 shows the detailed segmentation process for an example ground truth segmentation. A region growing method [15] is used to remove the background in Fig. 2a. Specifically, a seed point $p(i,j)$ which is manually selected is grown by searching the neighboring pixels. If the pixels meet $\mid p(i,j) - \mu_{RG} \mid \leq 2 \times \sigma_{RG}$, where $\sigma_{RG} = \sqrt{\sum_{i,j}^{N}(p(i,j) - \mu_{RG})^2/(N-1)}$, N is a small window, $\mid p(i,j) - \mu_{RG} \mid$ is the Euclidean distance between the color pixel $p(i,j)$ and the average color value μ_{RG} in RGB color space, the pixels are merged into the growing region. The processing will be stopped when there are no more pixels being added. Since the background maybe complicated, the seed points should be carefully selected in many different areas in order to make sure most of the background can be selected. Subsequently, the selected background is removed and filled as black (see Fig. 2b). In Fig. 2c, some regions in Fig. 2b which can not easily selected (such as the white color in Fig. 2b) are removed in this step. A specific color range is defined to remove the pixels which are similar to white color. Subsequently, morphology is used to fill the small gaps in the cell nuclei. Then a binary image shown in Fig. 2d is generated by using the pixels of which the color values are above zero. In Fig. 2e, Photoshop [16] is used to fuse the previous results and the original image. Then the cell nuclei boundaries are manually refined by visual contrast. Fig. 2f shows the final ground truth segmentation given by an expert. This artificial interactive segmentation method aims to help experts to reduce the segmentation time and the degree of complexity of the segmentation process.

3.1 Segmentation Results

In the segmentation processing, morphology is used to initial segment the cell nuclei. The radius of the disk structuring element for morphology opening and closing is 50 and 100, respectively. According to morphology segmentation results, the mean grey level value $\mu_{cellnuclei}$ and the standard deviation $\sigma_{cellnuclei}$ are calculated. Then the threshold T in Eq. 4 and σ in Eq. 5 can be estimated. In Eq. 4, $k = 0.5$. In Eq. 5, $\xi = 0.1$. Subsequently, the adaptive active contour modelling is used to segment the cell nuclei. In Eq. 2, $\lambda_1 = \lambda_2 = 10$. In the Split Bregman algorithm, $\Psi = 10^{-6}$, $1 < k < 30$. Fig. 3 shows some examples of segmentation results with the zoomed in images within the green rectangle regions. Compared with the ground truth, the boundaries of some cell nuclei are not convex for the results in [10]. This is partly explained by the fact that this method can not adapt to the grey level information for different kind of cell nuclei but could also be affected by the σ in Eq. 2. Compared with [10], the cell nuclei boundaries obtained by using the proposed method are smoother and perform better with the density inhomogenity.

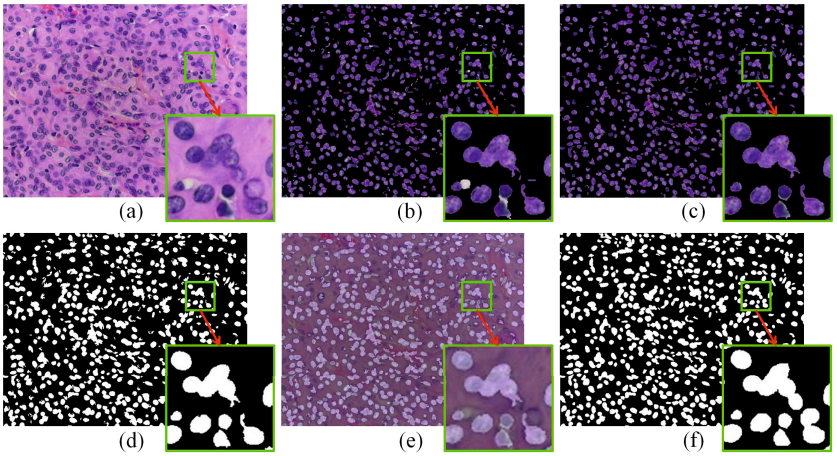

Fig. 2. Examples of ground truth segmentations. (a) original image, (b) region growing, (c) false positive removing by using color information, (d) morphology, (e) manually refinement by using Photoshop, (f) manual segmentation results.

To evaluate the accuracy of the segmentation results, two measures (true positive rate (TPR) and Dice similarity coefficient (DSC)) are used to evaluate the spatial accuracy of a segmentation result compared with the results of state-of-art methods [10]. The first measurement is defined as $TPR = TP/(TP+FN)$, where TP and FN are true positives and false negatives, respectively. The second measure is defined as $DSC(R1, R2) = (2 \times (R1R2))/((R1 + R2))$ which is used to measure the area overlap of the segmentation result (R1) with the ground truth masks (R2). These measurements have values in the range 0 to 1, where $TPR = 1$ or $DSC = 1$ indicates exact overlap with the ground truth, hence optimal segmentation. Tab. 1 shows the segmentation accuracy on each image, the overall mean and standard deviation for all the cases. Compared with state-of-art segmentation method [10], our results show improvements with the overall mean and standard deviation.

Table 1. TPR and Dice index for cell nuclei segmentation

Cell nuclei image	Active contour modelling [10]		Our results	
	TPR	DSC	TPR	DSC
Image 1	0.72	0.81	0.88	0.86
Image 2	0.72	0.78	0.84	0.82
Image 3	0.94	0.89	0.93	0.89
Image 4	0.75	0.84	0.85	0.87
Image 5	0.75	0.84	0.88	0.88
Overall mean	0.78	0.83	0.88	0.86
Standard deviation	0.09	0.04	0.04	0.03

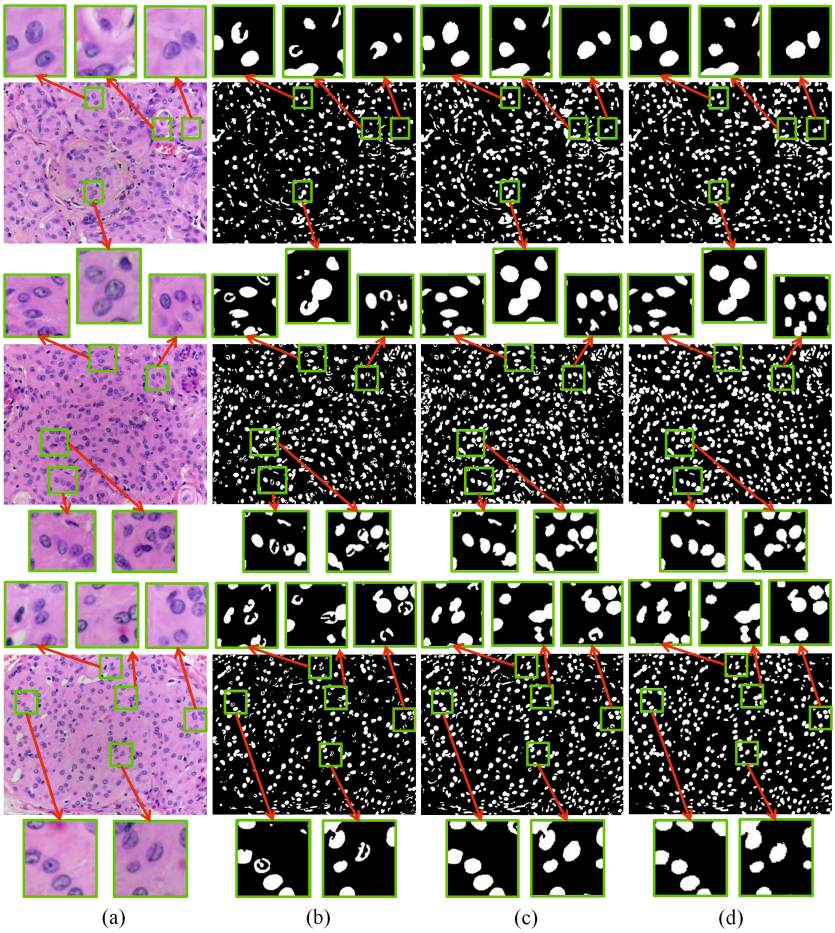

Fig. 3. Examples of the segmentation results. (a) original image, (b) active contour modelling [10], (c) our result, (d) ground truth.

4 Conclusions and Future Work

This paper presents a novel cell nuclei segmentation scheme based on morphology and adaptive active contour modelling. Also, an artificial interactive segmentation method is proposed to generate the ground truth for the evaluation. Our method has the following advantages. Firstly, the morphology results form the initialisation for the active contour modelling which can achieve the purpose of adaptive segmentation of the cell nuclei. Secondly, it can deal well with the density inhomogenity within the cell nuclei, and the segmentation results are more accurate and robust than the state-of-art method [10]. In the future, we will further evaluate our method on larger clinical datasets which included a variety of cell nuclei. In addition, cell nuclei splitting will be investigated to deal with the overlap of cell nuclei.

References

1. Sahoo, P.K., Soltani, S., Wong, A.K.C.: A survay of thresholding techniques. Computer Vision, Graphics, and Image Processing 41(2), 233–260 (1988)
2. Lee, K.M., Street, W.N.: An adaptive resource-allocating network for automatic detection, segmentation, and classification of breast cancer nuclei topic area: image processing and recognition. IEEE Transaction on Neural Network 14(3), 680–687 (2003)
3. Ruberto, C.D., Dempster, A., Kan, S., Jarra, B.: Analysis of infected blood cell images using morphological operators. Image and Vision Computing 20, 133–146 (2002)
4. Hu, M., Ping, X., Ding, Y.: Automated cell nucleus segmentation using improved snake. In: Proceedings of the International Conference on Image Processing, pp. 2737–2740 (2004)
5. Gurcan, M.N., Pan, T., Shimada, H., Saltz, J.: Image analysis for neuroblastoma classification: segmentation of cell nuclei. In: Proceedings of the 28th IEEE EMBS Annual International Conference, pp. 4844–4847 (2006)
6. Yang, F., Mackey, M.A., Ianzini, F., Gallardo, G., Sonka, M.: Cell segmentation, tracking, and mitosis detection using temporal context. In: Duncan, J.S., Gerig, G. (eds.) MICCAI 2005. LNCS, vol. 3749, pp. 302–309. Springer, Heidelberg (2005)
7. Zhang, B., Zimmer, C., Olivo, M.J.C.: Tracking fluorescent cells with coupled geometric active contours. In: Proceedings of the IEEE International Symposium on Biomedical Imaging: Nano to Macro, pp. 476–479 (2004)
8. Yang, L., Meer, P., Foran, D.J.: Unsupervised segmentation based on robust estimation and color active contour models. IEEE Transactions on Information Technology in Biomedicine 9(3), 475–486 (2005)
9. Li, C., Kao, C., John, C., Ding, Z.: Minimization of Region-Scalable Fitting Energy for Image Segmentation. IEEE Transactions on Image Processing 17(10), 1940–1949 (2008)
10. Yang, Y., Li, C., Kao, C.-Y., Osher, S.: Split bregman method for minimization of region-scalable fitting energy for image segmentation. In: Bebis, G., Boyle, R., Parvin, B., Koracin, D., Chung, R., Hammound, R., Hussain, M., Kar-Han, T., Crawfis, R., Thalmann, D., Kao, D., Avila, L. (eds.) ISVC 2010, Part II. LNCS, vol. 6454, pp. 117–128. Springer, Heidelberg (2010)
11. Goldstein, T., Bresson, X., Osher, S.: Geometric Applications of the Split Bregman Method: Segmentation and Surface Reconstruction. Journal of Scientific Computing 45, 272–293 (2010)
12. Haralick, R., Sternberg, S., Zhuang, X.: Image analysis using mathematical morphology. IEEE Transactions on Pattern Analysis and Machine Intelligence 9(4), 532–550 (1987)
13. Chan, T.F., Esedoglu, S., Nikolova, M.: Algorithms for finding global minimizers of denoising and segmentation models. SIAM Journal on Applied Mathematics 66, 1632–1648 (2006)
14. Bresson, X., Esedoglu, S., Vandergheynst, P., Thiran, J., Osher, S.: Fast Global Minimization of the Active Contour/Snake Model. Journal of Mathematical Imaging and Vision 28, 151–167 (2007)
15. Robb, R.: Biomedical imaging, visualization, and analysis. Wiley-Liss, USA (2000)
16. Adobe photoshop, `http://en.wikipedia.org/wiki/Adobe_Photoshop`